Proceedings of the ASME 2010 3rd Joint US-European Fluids Engineering Summer Meeting and 8th International Conference on Nanochannels, Microchannels, and Minichannels
FEDSM-ICNMM2010
August 1-5, 2010, Montreal, Canada

FEDSM-ICNMM2010-30068

NUMERICAL SIMULATIONS ON GAS-LIQUID-PARTICLE THREE-PHASE FLOWS UNDER MICROGRAVITY

Xinyu Zhang
Department of Mechanical and Aeronautical Engineering
Clarkson University, Potsdam, NY 13699-5725
The United States
zhangxi@clarkson.edu

Goodarz Ahmadi
Department of Mechanical and Aeronautical Engineering
Clarkson University, Potsdam, NY 13699-5725
The United States
ahmadi@clarkson.edu

ABSTRACT

Three-phase gas-liquid-particle flows under microgravity condition were numerically studied. An Eulerian-Lagrangian computational model was used in the simulations. In this approach, the liquid flow was modeled by a volume-averaged system of governing equations, whereas motions of particles and bubbles were evaluated using the Lagrangian trajectory analysis procedure. It was assumed that bubble shape variations were neglected and the bubbles remained spherical. The bubble-liquid, particle-liquid and bubble-particle interactions were accounted for in the analysis. The discrete phase equations included drag, lift, buoyancy, and virtual mass forces. Particle-particle interactions and bubble-bubble interactions were accounted for by the hard sphere model. Bubble coalescence was also included in the model. The transient flow characteristics of the three-phase flow were studied. The effects of gravity and g-jitter acceleration on variation of flow characteristics were discussed. The low gravity simulations showed that most bubbles are aggregated in the inlet region and the bubble plume exhibits a plug type flow behavior. The particles are mainly located outside the bubble plume, with very few particles being retained in the plume. Compared to the normal gravity condition, the three phases in the column are poorly mixed under microgravity conditions. The velocities of the three phases were also found to be of the same order. The simulation results showed that the effect of g-jitter acceleration on the gas-liquid-particle three phase flows is small.

Keywords: Three-Phase; Gas-Liquid-Particle; Numerical Simulation; Eulerian-Lagrangian Method; Microgravity; G-jitter acceleration.

INTRODUCTION

Three-phase liquid-gas-solid flows have broad applications in industrial processes (Fan, 1989), including three-phase slurry reactors in synthetic liquid fuel production. A thorough understanding of multiphase hydrodynamics is indispensable for optimization of three-phase slurry reactors. However, despite a number of studies, three-phase slurry reactor technology is far from being mature. In particular, while three-phase slurry reactors are expected to be key facilities for air revitalization and air purification for long duration human space travel, the three-phase flow characteristics under microgravity conditions are still not well understood yet.

Three phase flow related studies are very limited. Gidaspow et al. (1994) reported a model for three-phase-slurry hydrodynamics. Grevskott et al. (1996) developed a two fluid model for three-phase bubble columns in cylindrical coordinates, they used a k-ε turbulence model is used to consider bubble-generated turbulence. Mitra-Majumdar et al. (1997) proposed a CFD model coupled with a k-ε model to describe the turbulence for three phase flows through a vertical column. Wu and Gidaspow (2000) performed simulations on gas-liquid slurry bubble column using the kinetic theory of granular flow. Padial et al. (2000) reported simulations of three-phase flows in a three-dimensional draft-tube bubble column with a finite-volume technique. Gamwo et al. (2003) published a CFD model for chemically active three-phase slurry reactor for methanol synthesis. Zhou et al. (2005) developed a second-order moment three-phase turbulence model for simulating gas–liquid–solid flows. These models are all based on Eulerian-Eulerian approach. Numerical studies on gas-liquid-solid flows using an Eulerian-Lagrangian model are much more limited. Zhang (1999) performed a series of simulations on three-phase flows using volume-of-fluid (VOF)

model for the liquid and the bubbles and Lagrangian approach for particles, with only a few bubbles involved. Bourloutski and Sommerfeld (2002) carried out simulations on dense gas-liquid-solid flows using standard k-ε turbulence model, without considering bubble coalescence, bubble-bubble collision and particle-particle collision. Zhang and Ahmadi (2005) developed a Eulerian-Lagrangian model for simulations of gas-liquid-solid flows, where the bubbles and particles were treated as the dispersed discrete phases. Two-way coupling between the continuous liquid phase and the particles and bubbles were considered, and interactions between particle-particle, bubble-bubble, and particle-bubble as well as bubble coalescence were also included. Recently, they (2007) simulated three-phase flows under variable gravity conditions using this model.

In this study, to obtain the detailed characteristics of the three-phase flow under microgravity, the earlier developed computational model by Zhang and Ahmadi (2005) was used and a sample case with normal gravity was also analyzed first, then the influences of the microgravity on the three-phase flow characteristics were studied. The study was performed on a pseudo-two-dimensional bubble column with rectangular cross-section. Where the thickness of the column is 2 cm, and bubbles and particle can only move in the height and width directions. Besides, the volume of the bubbles and particles are considered as the volume of spheres. This simplification will save lots of computer resources, but may overestimate the discrete phase collisions in the height and width directions. Figure 1 shows the schematics of the bubble column. Bubbles rise through a 25 cm wide, 75cm high and 2cm thick column from 14 uniformly spaced gas inlets located in the center of the column bottom surface. The distance between every two neighboring inlet is 4mm. In the simulations, identical geometry was used and neutrally buoyant particles were randomly distributed in the column at the initial time. The continuous phase was assumed to be tap water. The initial liquid level is 55cm high, while the gravity is varied for different cases. Table 1 summarizes the hydrodynamic properties of the dispersed phases for different cases studied. Particle diameter and density are 0.25mm and 1000 kg/m^3, respectively.

NOMENCLATURE

C_D drag coefficient (dimensionless)

d_b bubble diameter (m)

d_p particle diameter (m)

d_d discrete phase diameter (m)

dt minimum time for next collision (s)

f_d coefficient used in drag coefficient calculation (dimensionless)

$\mathbf{F_b}$ buoyant force (N)

$\mathbf{F_d}$ drag force (N)

F_{Int} Interaction force (N)

$\mathbf{F_l}$ Saffman force (N)

$\mathbf{F_{vm}}$ virtual mass force (N)

g acceleration due to gravity force (ms^{-2})

I unit matrix

m_d discrete phase mass (kg)

P momentum transferred from the discrete phase (Nkg^{-1})

P pressure (Nm^{-2})

Re fluid phase Reynolds number (dimensionless)

Re_d discrete phase Reynolds number (dimensionless)

$\mathbf{u_d}$ fluid phase average velocity (ms^{-1})

$\mathbf{u_f}$ discrete phase velocity (ms^{-1})

U_s Superficial gas velocity

Greek letters

α_d phase coefficient (dimensionless)

Δt time step for liquid phase calculation (s)

ε_f liquid phase volume fraction (dimensionless)

λ_f liquid bulk viscosity (kgm^{-1}s^{-1})

μ_f liquid viscosity (Pas)

ρ_d discrete phase density (kgm^{-3})

ρ_f liquid phase density (kgm^{-3})

$\boldsymbol{\tau_f}$ fluid phase viscous stress tensor (Nm^{-2})

$\boldsymbol{\omega_f}$ liquid vorticity (s^{-1})

Table 1. Hydrodynamic parameters

Case number	Bubble diameter mm	Superficial gas velocity mm/s	Gravity m/s^2
1	1.0	0.25	-9.8
2	1.0	0.25	0.0
3	3.0	6.75	0.0
4	3.0	6.75	G-jitter

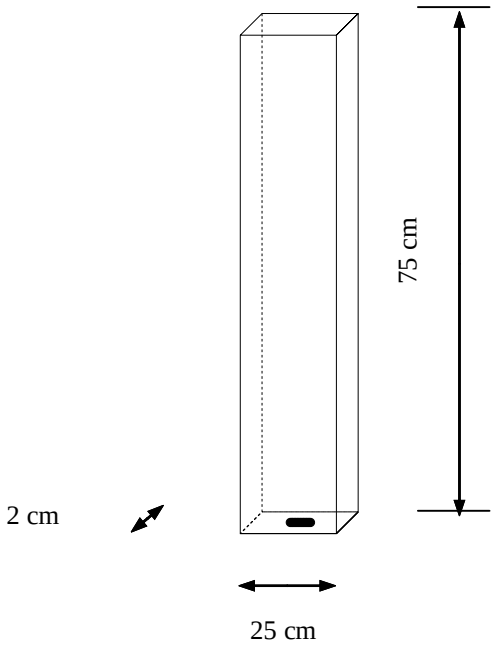

Figure 1. Sketch of the flat bubble columns (in cm)

Governing Equations and Models

The detailed information on governing equations and model assumptions were given by Zhang and Ahmadi (2005). Thus only the key equations are listed here.

Fluid Phase Hydrodynamics

The liquid phase is described by volume averaged, incompressible, transient Navier-Stokes equations. The volume-averaged continuity equation and momentum equation are given as

$$\frac{\partial(\varepsilon_f \rho_f)}{\partial t} + \nabla \cdot (\varepsilon_f \rho_f \mathbf{u_f}) = 0 \qquad (1)$$

$$\rho_f \varepsilon_f \frac{d(\mathbf{u_f})}{dt} = -\varepsilon_f \nabla p + \nabla \cdot (\varepsilon_f \boldsymbol{\tau}_f) + \rho_f \mathbf{g} \varepsilon_f + \mathbf{P} \qquad (2)$$

Here, ε_f is the liquid phase volume fraction, ρ_f is the liquid phase density, $\mathbf{u_f}$ is the fluid phase average velocity, p is pressure, g is the acceleration of gravity, P is interaction momentum per unit mass transferred from the discrete phases , and $\boldsymbol{\tau}_f$ is the liquid phase viscous stress tensor, which is given by

$$\boldsymbol{\tau}_f = -\frac{2}{3}\mu_f (\nabla \cdot \mathbf{u_f}) I + \mu_f \left((\nabla \mathbf{u_f}) + (\nabla \mathbf{u_f})^T \right) \qquad (3)$$

where μ_f is the liquid viscosity.

Dispersed Phase Dynamics

The bubbles and particles are treated as discrete phases and their motions are governed by Newton's second law.:

$$m_d \frac{d\mathbf{u_d}}{dt} = \mathbf{F_d} + \mathbf{F_b} + \mathbf{F_{vm}} + \mathbf{F_l} + \mathbf{F_{Int}} \qquad (4)$$

Where m_d and $\mathbf{u_d}$ are mass and the discrete phase velocity respectively. The terms on the right hand side of Equation (6) are, respectively, drag, buoyancy, virtual mass, lift and interaction forces. The interaction force F_{Int} includes particle-particle, bubble-bubble and particle-bubble collisions.

The drag force, $\mathbf{F_d}$, is given by

$$\mathbf{F_d} = \begin{cases} 0.125 \rho_f C_D \pi d_d^2 |\mathbf{u_f} - \mathbf{u_d}| (\mathbf{u_f} - \mathbf{u_d}), & Re_d \geq 1 \\ \alpha_d \pi \mu_f d_d (\mathbf{u_f} - \mathbf{u_d}), & Re_d < 1 \end{cases} \qquad (5)$$

Where d_d is the discrete phase diameter, α_d is a phase coefficient whose value is 2 for bubble and 3 for rigid particle to account for the variation of the Stokes drag force for bubbles and particles in low Reynolds number flows. In Equation (5), Re_d is the discrete phase Reynolds number defined by

$$Re_d = \rho_f d_d \frac{|\mathbf{u_f} - \mathbf{u_d}|}{\mu_f} \qquad (6)$$

C_D is the drag coefficient given as

$$C_D = f_d \frac{24}{Re_d} \qquad (7)$$

Where, f_d is given by

$$f_d = \begin{cases} 1 + 0.15 Re_d^{0.687}, Re_d \leq 1000 \\ 0.0183 Re_d, Re_d > 1000 \end{cases} . \qquad (8)$$

$\mathbf{F_l}$ in Equation (4) is the Saffman lift force given by

$$\mathbf{F_l} = 1.61 d_d^2 (\mu_f \rho_f)^{0.5} |\boldsymbol{\omega_f}|^{-0.5} [(\mathbf{u_f} - \mathbf{u_d}) \times \boldsymbol{\omega_f}], \qquad (9)$$

In which, flow vorticity $\boldsymbol{\omega_f}$ is defined as

$$\boldsymbol{\omega_f} = \nabla \times \mathbf{u_f} . \qquad (10)$$

$\mathbf{F_b}$ in Equation (4) is the buoyant force given by:

$$\mathbf{F_b} = \frac{\pi d_d^3}{6} (\rho_f - \rho_d) \mathbf{g} \qquad (11)$$

Where ρ_d is the discrete phase density.

$\mathbf{F_{vm}}$ in Equation (4) is the virtual mass force given by

$$\mathbf{F_{vm}} = -\frac{1}{12}\pi d_d^3 \rho_f \frac{d}{dt}(\mathbf{u_d} - \mathbf{u_f}) \quad (12)$$

Discrete Phase Collisions and Two-Way Coupling

Bubble-bubble and particle-particle collisions are included in this study by using a hard sphere collision model originally developed by Hoomans et al. (1996). However, the effects of the rotation of bubbles and particles were neglected in the analysis. Restitution coefficients of 0.2 for bubble-bubble collision and 0.5 for particle-particle collision are used. Friction coefficients of 0.02 and 0.1 are assumed for bubbles and particles and all the bubble-bubble and particle-particle collisions are assumed binary.

Bubble-particle interactions are included in the study by assuming the particles always go through the bubbles when bubble–particle collision happens. Multi-interactions between bubble and particle are considered in this model, which means at the same time, more than one particle can enter the same bubble or different bubbles. Bubble coalescence is also included by assuming that two bubbles coalesce upon impact when the Weber number less than 0.14, while they bounce back for larger Weber numbers.

Two-way fluid-dispersed phase coupling is implemented through momentum interaction term, P, from the discrete phase to fluid phase. P is the negative of the sum of all forces acting on the particles and bubbles exerted by the fluid in a certain Eulerian cell. The coupling between bubbles and particles is implemented through bubble-particle interactions. When a particle enters a bubble, all the forces acting on the particles by the new gaseous environment are calculated using the bubble hydrodynamic properties till the particle leaves the bubble. The exact force with opposite direction is then added to the bubble equation of motion.

Boundary Conditions

No-slip boundary conditions were used on the walls of the column for the liquid phase and an outflow condition was assumed at the upper boundary of the column. Bubble-wall and particle-wall collisions were included by a hard sphere model revised from the model developed by Hoomans et al. (1996). The wall roughness effects and the rotation of bubbles and particles were ignored. A restitution coefficient of 0.5 was used for both bubble-wall collision and particle-wall collision. Friction coefficients of 0.02 and 0.1 were used for bubble-wall collision and particle-wall collision, respectively.

The marker-and-cell (MAC) method (Harlow and Welch, 1965) was used to simulate the column free surface. Interaction of bubbles with the free surface is included by assuming that the bubbles impacting the column free surface with Weber number less than 0.28 will break and leave the column, while bubbles impacting at higher Weber numbers will bounce back using a hard sphere model. A Restitution coefficient of 0.2 was used for bubble-free surface collisions for We > 0.28.

Numerical Procedure

The governing equations were discretized with finite difference method in a structured equidistant staggered grid. A combination of central and donor-cell discretization scheme was used for convective parts, while an explicit time step was used for time updating. The model was implemented in a new developed computer code ELM3PF (Eulerian-Lagrangian Method for Three Phase Flow) for simulation of three phase flows. The new code was developed in C from NaSt2D code, which was a code for single-phase flows with free surface developed by Griebel et al. (1998). ELM3PF can be used to simulate unsteady, two-dimensional three-phase liquid-gas-solid flows with free surface.

In ELM3PF, the pressure Poisson equations for liquid phase are solved by successive over-relaxation (SOR) method. A fixed time step, Δt, which is 0.001s, is used for liquid phase calculation in the study. After obtaining the new liquid velocity field, the code evaluates the minimum time for next collision, dt, which is the minimum time of all possible collisions. If dt is smaller than Δt, the code calculates bubble and particle velocities and positions over the time duration dt. The next collision process is then analyzed, and the corresponding discrete phase velocities after the collision are evaluated. Then the code computes the next minimum time for collision and repeats this procedure until the accumulation of these dt equals Δt. Thereafter the forces acting on the bubbles and particles are evaluated and transferred into the momentum equation for the liquid phase. The code then computes the new liquid velocity field. If minimum collision time dt is larger than Δt, the code compute the forces acting on the bubbles and particles, and then transfer these forces into momentum equations for liquid phase and evaluates the new liquid velocity. For a typical number of 9940 bubbles and 1000 particles with a computational grid of 1500 cells, evaluation of one second transient behavior of the liquid-gas-solid three-phase flow requires around 4 hours CPU time on a SUN Ultra10 workstation.

Effect of Grid Size

To test the sensitivity of the simulation result on the grid size, the grid size was reduced from 1cm to 0.5cm. The results of the two cases did not show obvious difference. Thus, a grid spacing of 1cm was typically used.

Results and Discussion

In this section the results are presented and discussed.

Development of Transient Flow Structures with Normal Gravity

In order to evaluate the effect of the microgravity on the three-phase flow characteristics, a sample reference case with normal gravity is studied first. The hydrodynamic parameters for the simulation are listed in Table 1 (case 1).

Figure 2 shows the snapshots of the predictions for the liquid

tracers, and the locations of bubbles and particles at time of 1, 9, 22 and 30 s after initiation of the flow. The small dots in Figure 2 show the liquid phase tracers, while the small circles and the large circles show, respectively, the positions of the particles and bubbles. Figures 3, 4 and 5, respectively, show the corresponding velocities of bubbles, liquid and particles. It can be seen from Figure 2a, 2b and 2c that bubble plume rises rectilinearly along the centerline of the column, and generates two vortices behind the plume head, as also seen in Figure 4a, 4b and 4c, these vortices are almost symmetric in early start time, but with the evolution of the flow, they gradually become non-symmetric, eventually staggered vortical flows are formed, as shown by Figure 4d. Due to these staggered vortices, the bubble plume changes its pattern to S-shape as seen in Figure 2d. With the pushing of the bubble plumes, the moving of these staggered vortices results in the oscillation of the bubble plume. Comparison of Figure 2 and Figure 4 shows that the evolution of the three-phase flow is controlled by these time-dependent staggered vortices, the expanding of the bubble plume on the top of the column and the shrinking on the bottom is also a result of the vortices.

It can be seen from Figure 3b, 3c and 3d that bubble upward velocities first increase along the column height, after attain the maximum, then decrease along the column height because of the increasing liquid drag resulted from the low liquid upward velocity at the free surface region. Comparison of Figure 3b, 3c and 3d shows that bubble maximum upward velocities increase with time, therefore the differences of the bubble upward velocities along the column height increase with time, which may result in more bubble-bubble collision and coalescence.

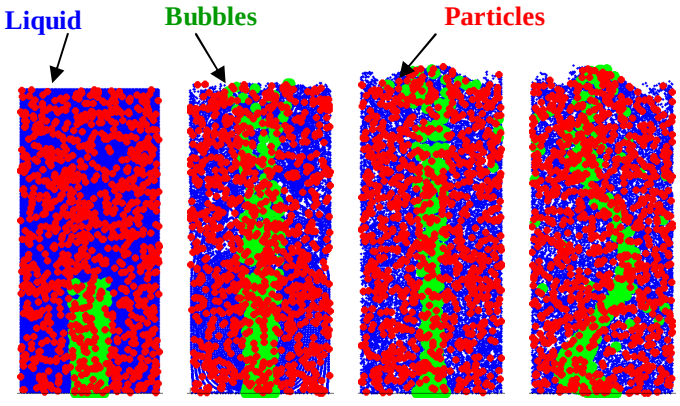

Figure 2. Computed flow structure of the gas-liquid-particle three-phase flow in normal gravity. Superficial gas velocity (U_s = 0.25mm/s, initial bubble size d_b = 1.0 mm)

Figure 4 and Figure 5 show that the liquid and particle upward velocities also first increase then decrease along the column height, which will result in more particle-particle collision with the development of the flow. Figure 4 also implies that due to the effect of liquid vortices, bubbles and particles in the low part of the column are pushed toward the centerline, which will result in horizontal bubble-bubble and particle-particle collisions. In the central region, particles and bubbles are in the upward acceleration process, particles or bubbles behind can not easily catch up those above them, so longitudinal collisions are scarce. While in the top part of the column, the liquid will push the bubbles and particles toward the side walls of the column, so horizontal collisions are scarce. However, particles and bubbles in this region are in the deceleration process, so longitudinal collisions will play a important role. As for the bubble-particles collisions, longitudinal collisions can happen along the full column height because the bubble upward velocities are in general larger than the particle upward velocities.

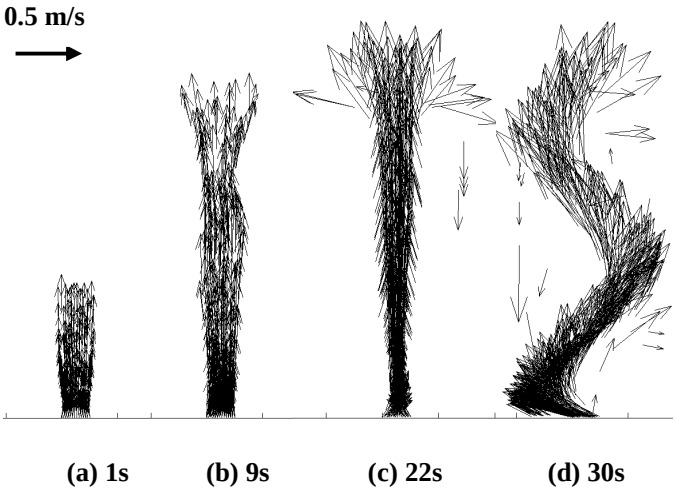

Figure 3. Computed snapshots of the bubble velocities of the gas-liquid-particle three-phase flow in normal gravity. Superficial gas velocity (U_s = 0.25 mm/s, initial bubble size d_b = 1.0 mm)

Comparison of Figures 2, 4 and 5 indicates that most particles are pushed away from the center of the vortices due to inertia and concentrated in the region outside the large vortices. However, some particles are retained inside these staggered vortices, partly because of particle-particle collisions.

Comparison of Figures 3, 4 and 5 indicates the bubble upward velocities are much larger than both particle and liquid velocities, but downward velocities of the captured bubbles are smaller than both particle and liquid velocities. The reason is that bubble upward buoyancy is the main driving force for the flow, so bubble upward velocities are much larger than both particle and liquid velocities. However, for downward velocities of the captured bubbles, bubbles are pushed downward by liquid velocity, while the bubble buoyant force is always upward, thus the bubble can not follow the liquid well, therefore the bubble

downward velocities are smaller then both particle and liquid downward velocities.

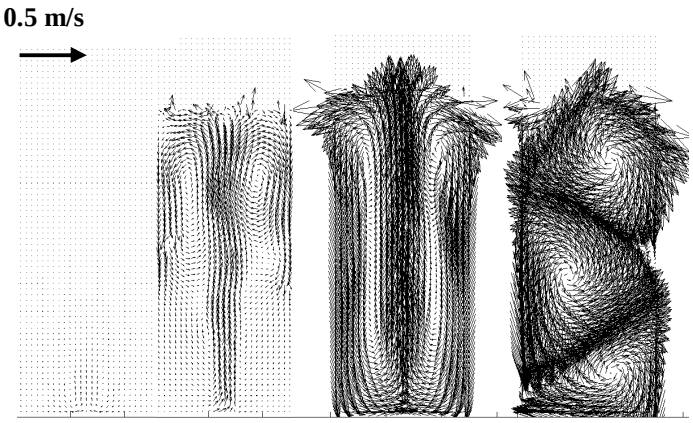

Figure 4. Computed snapshots of the liquid velocities of the gas-liquid-particle three-phase flow in normal gravity. Superficial gas velocity (U_s = 0.25 mm/s, initial bubble size d_b = 1.0 mm)

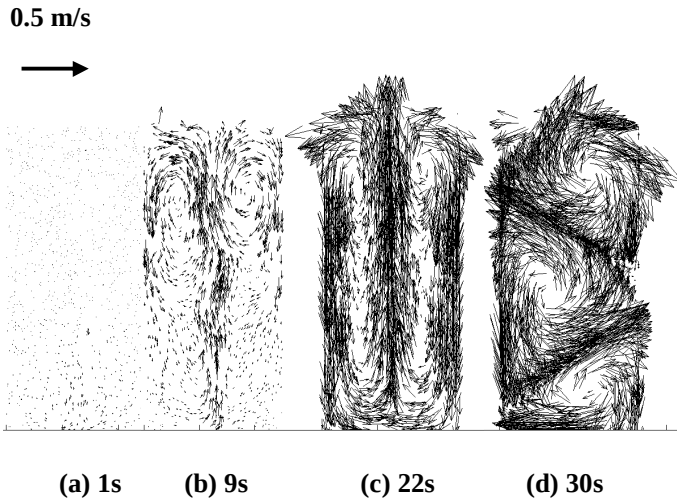

Figure 5. Computed snapshots of the particle velocities of the gas-liquid-particle three-phase flow in normal gravity. Superficial gas velocity (U_s = 0.25 mm/s, initial bubble size d_b = 1.0 mm)

Figures 4 and 5 show that velocities of particles and liquid are in the same order, but because particles are neutrally buoyant and are generally transported by the liquid, particle velocity is generally slightly smaller than the liquid velocities. While if particles with high velocities entrain in low liquid velocity regions, the particle local velocities may become slightly larger than the liquid phase.

Development of Transient Flow Structures in Zero-Gravity

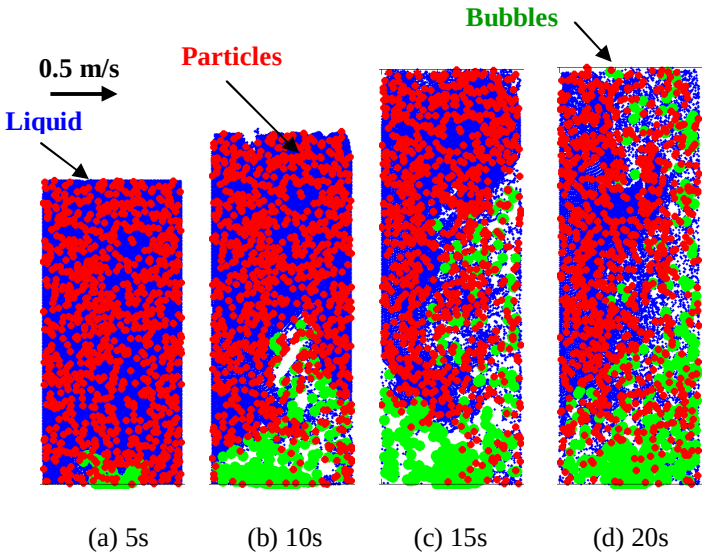

Figure 6. Computed flow structure of the gas-liquid-particle three-phase flow in zero-gravity. (Superficial gas velocity U_s = 0.25 mm/s, initial bubble size d_b =1.0 mm)

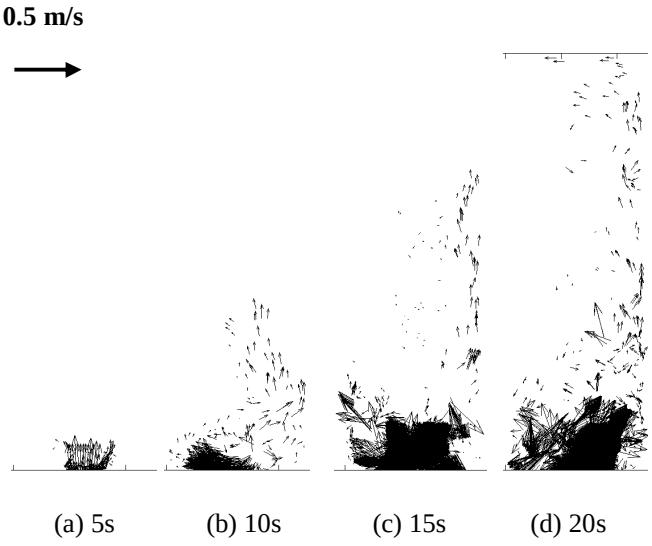

Figure 7. Computed snapshots of the bubble velocities of the gas-liquid-particle three-phase flow in zero-gravity. (Superficial gas velocity U_s = 0.25 mm/s, initial bubble size d_b =1.0mm)

In order to study the effect of gravity on the three-phase flow, a study of the characteristics of three-phase liquid-gas-solid flows under zero-gravity condition is given in this section. The

hydrodynamic parameters used in the simulation are listed in Table 1 (case 2). Figure 6 shows the snapshots of the model predictions for the liquid tracers and the locations of bubbles and particles at the time of 5, 10, 15 and 20 s after initiation of the flow. Figures 7, 8 and 9 show the corresponding bubble velocities, liquid velocities and particle velocities, respectively. Under zero-gravity, there is no buoyant force acting on the bubbles or the particles. Bubble motions are originated from the bubble initial injection momentum, and affected by bubble-bubble collisions, bubble-particle collisions, and liquid drag. Thus, compared to the flow with normal gravity, bubbles move very slowly in the column under zero-gravity condition.

It can be seen from Figure 6a that bubbles do not rise rectilinearly under zero-gravity condition. The reason is when bubbles enter the column, they quickly lose their initial momentum due to the liquid drag, and accumulate at the bottom of the column due to the lack of buoyant force. When a sufficient number of bubbles is reached, they start to rise due to bubble-bubble collision and liquid movement. Figures 6a and 9a show that particles are pushed away when the bubble clusters raise. Figures 6b and 6c show the significant increase of the liquid level in the column with time, which is due to the accumulation of a large number of bubbles in the column in zero-gravity condition. Figures 6b, 7b, and 8b show a plug flow behavior with the liquid above the bubble clusters moving with a roughly uniform velocity. When the bubble plume reaches the free surface, a large vortex is formed as shown in Figures 6d, 7d and 8d. Figures 6 and 9 also show that most particles are located in the region outside the bubble plume, with only a few particles retained inside the plume.

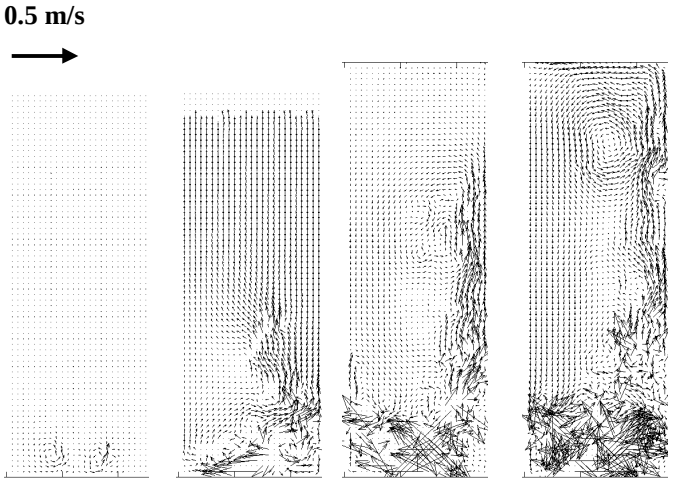

(a) 5s (b) 10s (c) 15s (d) 20s

Figure 8. Computed snapshots of the liquid velocities of the gas-liquid-particle three-phase flow in zero-gravity. (Superficial gas velocity U_s = 0.25mm/s, initial bubble size d_b = 1.0mm)

Comparison of Figures 7, 8 and 9 indicates that the velocities of bubbles, liquid and particles are of the same order under the zero-gravity condition, especially at the top of the column. There is exception for the startup when the bubble upward velocities are much larger than both liquid and particle velocities.

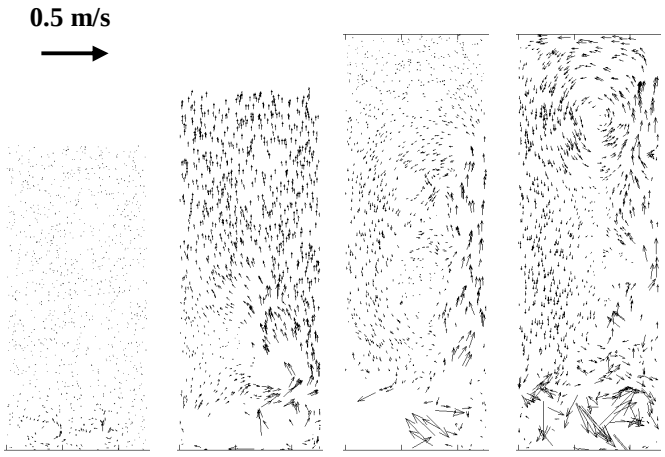

(a) 5s (b) 10s (c) 15s (d) 20s

Figure 9. Computed snapshots of the particle velocities of the gas-liquid-particle three-phase flow in zero-gravity. (Superficial gas velocity U_s = 0.25 mm/s, initial bubble size d_b = 1.0 mm)

Comparing Figures 6, 7, 8 and 9, respectively, with Figures 2, 3, 4 and 5 shows the significant effect of gravity on the three-phase flow characteristics. Clearly, bubble rising velocities are very small due to the lack of buoyant force. Also because many bubbles are accumulated in the column, the liquid level in the column at zero-gravity is much higher than that of the flow with normal gravity. Besides, because most particles are located in the region outside the bubble plume, the mixing of different phases is much less when compared with that for the flow with normal gravity. Thus, the interactions among the different phases are significantly reduced under zero-gravity condition. Compared to Figures 4 and 5, Figures 8 and 9 show that both liquid and particle velocities are smaller than those of the flow with normal gravity. In summary, compared with the flow in normal gravity, the flow in zero-gravity has low phase velocity and phase mixing.

Effect of Bubble Size on Gas-Liquid-Particle Flow in Zero-gravity

To study the effect of bubble size on the flow characteristics under zero-gravity, the simulation was repeated with the inlet bubble diameter increased to 3mm and superficial velocity increased to 6.75mm/s, which maintained the same number of bubble injections at the inlet. Other simulation parameters are

the same as those listed in Table 1 (case 3). Figure 10a shows the flow structures at 6 s after initiation of the three-phase flow. Figures 10b, c and d show the corresponding velocities of bubbles, liquid, and particles, respectively.

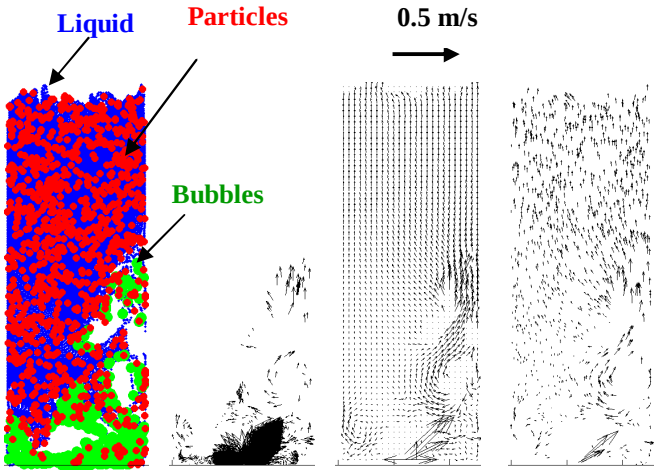

Figure 10. Computed flow structure and velocities of the gas-liquid-particle three-phase flow in zero-gravity. Superficial gas velocity U_s = 6.75 mm/s, initial bubble size d_b = 3.0 mm.

Compared to Figures 6a and 7a, Figures 10a and 10b show that larger bubbles have larger upward velocities due to increased buoyant force; thus, the bubble plume evolves faster than that with smaller inlet bubbles. Comparisons of Figure 8a and Figure 10c, as well as Figure 9a and Figure 10d, indicate that both liquid and particle velocities with larger inlet bubbles are higher than those velocities with smaller inlet bubbles. This can be explained by bubble inertia and the momentum transferred among the three phases. Since the number of injected bubbles is fixed, larger bubbles imply larger superficial velocity, which indicates that in the same time period larger bubble momentum is introduced into the column and transferred to the liquid and particle phases. Thus, the liquid and particle velocities in the column are higher than those with smaller injected bubbles.

Effect of g-jitter Acceleration on Gas-Liquid-Particle Flow in Zero-gravity

To study the effect of g-jitter acceleration on the gas-liquid-particle three-phase flow characteristics under zero-gravity, a simulation was performed under g-jitter acceleration from STS-51 data. The simulation parameters are listed in case 4 of Table 1. Figure 11 shows the variation of g-jitter acceleration with time from STS-51 data. It can be seen from Figure 11 that g-jitter acceleration is very small compared to the acceleration of normal gravity. In the simulation, the g-jitter acceleration is added in the equation of motion of the liquid phase as the body force acceleration. Figure 12a shows the flow structures at 6 s after initiation of the three-phase flow under g-jitter acceleration. Figures 12b, c and d show the corresponding velocities of bubbles, liquid, and particles, respectively. Compared to Figure 10, Figure 12 shows a little bit more uniformly distributed bubbles due to the shaking effect of g-jitter acceleration, but the differences are small, which implies that the effect of g-jitter acceleration on the gas-liquid-particle three-phase flows is small.

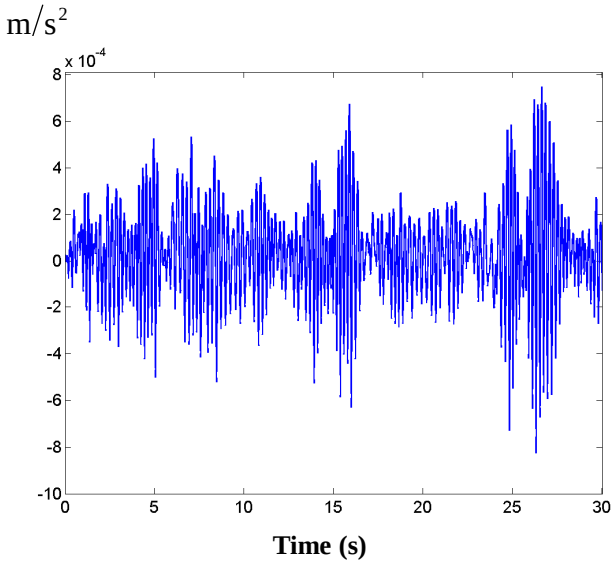

Figure 11. The variation of G-jitter acceleration with time from STS 51 data.

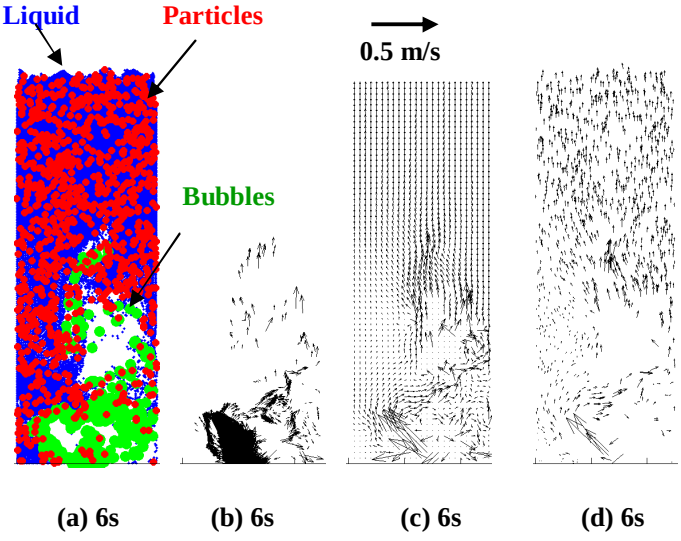

Figure 12. Computed flow structure of the gas-liquid-particle three-phase flow in zero-gravity with G-jitter. Superficial gas velocity U_s = 6.75 mm/s, initial bubble size d_b = 3.0 mm.

CONCLUSIONS

In this study, an Eulerian-Lagrangian computational model for simulations of gas-liquid-solid flows in microgravity is presented. The two-way couplings between bubble-liquid and particle-liquid were included in the analysis. Interactions between particle-particle and bubble-bubble as well as the bubble coalescence were also included. The transient characteristics of three-phase flows in zero-gravity and microgravity were studied and the effects of gravity, bubble size and g-jitter acceleration on the characteristics of the flow were discussed. On the basis of the presented results, the following conclusions are obtained:

1. Gravity has a significant influence on the transient characteristics of the flow in the bubble column. In the flow without gravity, the sources for bubble motion are mainly bubble initial momentum, bubble-bubble collision and liquid transportation. Thus bubbles accumulate at the bottom of the column and move very slowly, as a result, the liquid level is much higher than that of the flow with normal gravity.
2. The flow in zero-gravity has low phase velocities and phase mixing. Besides, in most region, the velocities of bubbles, liquid and particles are in the same order.
3. Bubble size has a major effect on the flow. Larger bubbles have larger velocities; thus the bubble plume evolves faster than that with smaller bubbles.
4. The effect of G-jitter acceleration on the gas-liquid-particle three-phase flows is small.

ACKNOWLEDGMENTS

The financial support by the US Department of Energy is gratefully acknowledged.

REFERENCES

Bourloutski, E. and Sommerfeld M., Transient Euler/Lagrange calculations of dense gas--liquid-solid flows in bubble column with consideration of phase interaction. 2002. Proceedings 10th Workshop on Two-Phase Flow Predictions, Merseburg, pp. 113-123.

Delnoij, E., J. A. M. Kuipers, and W. P. M. van Swaaij, 1997, Dynamic simulation of gas-solid two-phase flow:effect of column aspect ratio on the flow structure, Chem. Eng. Sci. **52**, 3759.

Fan, L.-S., 1989, Gas-Liquid-Solid Fluidization Engineering, Butterworths, Boston.

Gamwo, I.K., Halow, J.S., Gidaspow, D., and Mostofi, R., 2003. CFD Models for Methanol Synthesis Three-Phas Reactors: Reactor Optimization, Chemical Engineering Science **93**, pp. 103-112.

Gidaspow, D., M. Bahary, and U.K. Jayaswal, 1994, Hydrodynamic models for gas-liquid-solid fluidization, Numerical Methods in Multiphase Flows, FED **185**,ASME, New York, NY, pp 117-124.

Grevskott, S., B. H. Sannas, M. P. Dudukovic, K. W. Hjarbo, and H. F. Svendsen, 1996, Liquid circulation, bubble size distributions, and solids movement in two- and three-phase bubble columns, Chem. Eng. Sci. **51**, 10, 1703.

Mitra-Majumdar, D., B. Farouk, and Y. T. Shah, 1997, Hydrodynamic modeling of three-Phase flows through a vertical column, Chem. Eng. Sci. **52**, 24, 4485.

Padial, N. T., W. B. VanderHeyden, R. M. Rauenzahn, & S. L. Yarbo, 2000. Three-Dimensional simulation of a three-phase draft-tube bubble column, Chem. Eng. Sci. **55**, 3261-3273.

Wu, Y., D. Gidaspow, 2000,Hydrodynamic simulation of methanol synthesis in gas-liquid slurry bubble column reactors, Chem. Eng. Sci. **55**, 573-587.

Zhang, J. P, 1999, Discrete phase simulation of bubble and particle dynamics in gas-liquid-solid fluidization systems, Ph.D. thesis, The Ohio State University.

Zhou, L., Yang, M. and Fan L., 2005. A second-order moment three-phase turbulence model for simulating gas–liquid–solid flows. *Chem. Eng. Sci*. **60**, pp. 647-653.

Zhang, X. and Ahmadi, G., 2005. Eulerian-Lagrangian simulations of liquid-gas-solid flows in three-phase slurry reactors. *Chem. Eng. Sci*. **60**, pp. 5089-5104.

Zhang, X. and Ahmadi, G., 2007. Simulations of Three-phase Liquid-Bubble-Solid Flows under Variable Gravitation Conditions, Proceedings of International Conference on Multiphase Flow, 9.-13. July, Leipzig,Germany.